Analytic derivatives of scaling motion-compensated projection operators for dynamic computed tomography

Anh-Tuan Nguyen[1], Jens Renders[1], Jeroen Soete[2], Martine Wevers[2], Jan Sijbers[1], Jan De Beenhouwer[1]

[1]imec-Vision Lab, Department of Physics, University of Antwerp, Antwerp, Belgium

Email: {anh-tuan.nguyen, jens.renders, jan.debeenhouwer, jan.sijbers}@uantwerpen.be

[2]Department of Materials Engineering, Katholieke Universiteit Leuven, Leuven, Belgium

Email: {jeroen.soete, martine.wevers}@kuleuven.be

Abstract

This work presents an iterative method in dynamic computed tomography (dynamic CT) which enables accurate reconstruction and scaling correction simultaneously. Recent achievements in dynamic CT have shown the feasibility of reconstructing an image of an object while simultaneously estimating its temporal deformation model parameters. Those approaches consider a mathematical minimization problem whose objective function depends on the reconstruction as well as on the deformation parameters corresponding to the motion model, mostly represented by affine transformations. Nonetheless, they lack a validation on non-rigid motion models wherein the motion is estimated by an objective function whose partial derivatives toward motion parameters are analytical. In this work, those operators are analytically given. Results from simulation and real data experiments show that the blurring artifacts caused by the motion are largely reduced.

Keywords: Dynamic computed tomography, scaling parameter estimation.

1 Introduction

Dynamic computed tomography (dynamic CT) is a sub-field of CT imaging which aims to capture the 3D structure of objects in motion. Its applications, including reconstruction and visualization, can be widely found not only in biomedical imaging but also in materials science. Examples include skins [1], fibre-reinforced composites [2], or more recently, carbon materials like diamonds [3]. Dynamic CT reconstruction techniques aim to improve resolution both in temporal and spatial domains.

Current techniques that combine reconstruction and deformation estimation in dynamic CT can be categorized into two classes. In the first class, the methods consider few restrictions on the deformation. Examples can be Total Variation Regularization (TVR) [4] which aims to learn sparsity in the spatial domain, or Spatial-temporal Total Variation Regularization (STTVR) [5] and Space-time Tomography [6], both developed from the TVR method by additionally optimizing the sparsity in the temporal domain. Apart from the sparsity, a modified SIRT algorithm with an intuitive interpretation is considered in the MotionVector-based Iterative Technique (MoVIT) [7]. A common point in all those methods is that they do not consider any deformation model. As a result, it is challenging to describe the deformation exactly. Another class of methods, which consider particular motion models, is characterized by a few unknown motion parameters. Examples range from simultaneous reconstruction and either rigid or non-rigid motion correction techniques [8, 9], to reconstruction and general affine-transformed deformation correction techniques [10, 11].

This work presents a novel dynamic reconstruction method that does not only deliver an accurate reconstruction but also estimates the motion more precisely than general affine-transformed deformations as in [10, 11]. The dynamic CT process is modelled as a linear system, whose system operator can be represented as a decomposition between the projector and motion operators. By minimizing the projection data fidelity term in the entire dynamic acquisition, the reconstruction and scaling parameters are obtained by a gradient method which aims to minimize an objective function that depends on both of them. The scaling-compensated projection operators are given analytically. Our method is validated both on simulated and real projection data.

2 Method

A 4D image can be interpreted as a multi-time series of n 3D images $\boldsymbol{x}_1, \boldsymbol{x}_2, \ldots, \boldsymbol{x}_n$, each representing the object at a given continuous time frame. In order to model this process mathematically, let us consider the following systems of linear equations:

$$\boldsymbol{W}_i \boldsymbol{x}_i = \boldsymbol{b}_i \text{ for } i = 1, 2, \ldots, n, \tag{1}$$

wherein $\boldsymbol{W}_i$ and $\boldsymbol{b}_i$ are respectively the corresponding projection operator and the projection data of the i^{th} time frame. These can be represented as follows:

$$\begin{bmatrix} \boldsymbol{W}_1 & 0 & 0 & 0 \\ 0 & \boldsymbol{W}_2 & 0 & 0 \\ 0 & 0 & \ddots & 0 \\ 0 & 0 & 0 & \boldsymbol{W}_n \end{bmatrix} \begin{bmatrix} \boldsymbol{x}_1 \\ \boldsymbol{x}_2 \\ \vdots \\ \boldsymbol{x}_n \end{bmatrix} = \begin{bmatrix} \boldsymbol{b}_1 \\ \boldsymbol{b}_2 \\ \vdots \\ \boldsymbol{b}_n \end{bmatrix}. \tag{2}$$

Let us assume that the unknown 3D image $\boldsymbol{x}_i$ of the i^{th} time frame is scaled from its unknown initial scaleless state $\boldsymbol{x}$ under a scaling model, which depends on the scaling parameter $\boldsymbol{s}_i = (s_{i,x}, s_{i,y}, s_{i,z})$, i.e,

$$\boldsymbol{x}_i(x,y,z) = \boldsymbol{x}(s_{i,x}x, s_{i,y}y, s_{i,z}z), \tag{3}$$

where (x,y,z) are the coordinates of the voxels of the image $\boldsymbol{x}_i$.

Let us denote M as the linear transformation that represents the scaling model introduced above, then equation (3) can be rewritten as follows:

$$\boldsymbol{x}_i = M(\boldsymbol{s}_i)\boldsymbol{x}. \tag{4}$$

By substituting (4) into (2) for all $i = 1,2,\ldots n$, we obtain the following dynamic CT model of the entire scan:

$$\begin{bmatrix} \boldsymbol{W}_1 & 0 & 0 & 0 \\ 0 & \boldsymbol{W}_2 & 0 & 0 \\ 0 & 0 & \ddots & 0 \\ 0 & 0 & 0 & \boldsymbol{W}_n \end{bmatrix} \begin{bmatrix} M(\boldsymbol{s}_1) \\ M(\boldsymbol{s}_2) \\ \vdots \\ M(\boldsymbol{s}_n) \end{bmatrix} \boldsymbol{x} = \begin{bmatrix} \boldsymbol{b}_1 \\ \boldsymbol{b}_2 \\ \vdots \\ \boldsymbol{b}_n \end{bmatrix}, \tag{5}$$

or in a more condensed notation:

$$\boldsymbol{W}\boldsymbol{M}(\boldsymbol{s})\boldsymbol{x} = \boldsymbol{b}. \tag{6}$$

The system (6) can be solved by using a gradient method which aims to minimize the following objective function:

$$f(\boldsymbol{x},\boldsymbol{s}) = \frac{1}{2}\|\boldsymbol{W}\boldsymbol{M}(\boldsymbol{s})\boldsymbol{x} - \boldsymbol{b}\|_2^2. \tag{7}$$

The partial derivatives of the objective function towards the reconstruction and motion parameters are given by

$$\nabla_{\boldsymbol{x}} f(\boldsymbol{x},\boldsymbol{s}) = \boldsymbol{M}(\boldsymbol{s})^T \boldsymbol{W}^T [\boldsymbol{W}\boldsymbol{M}(\boldsymbol{s})\boldsymbol{x} - \boldsymbol{b}], \tag{8}$$

$$\nabla_{\boldsymbol{s}} f(\boldsymbol{x},\boldsymbol{s}) = [\nabla \boldsymbol{M}(\boldsymbol{s})\boldsymbol{x}]^T \boldsymbol{W}^T [\boldsymbol{W}\boldsymbol{M}(\boldsymbol{s})\boldsymbol{x} - \boldsymbol{b}]. \tag{9}$$

The motion operator $\boldsymbol{M}(\boldsymbol{s})$, its conjugate $\boldsymbol{M}(\boldsymbol{s})^T$ and its partial derivative towards the scaling parameters $\nabla\boldsymbol{M}(\boldsymbol{s})$ are all provided by an in-house implementation of cubic image warping [12]. The projector $\boldsymbol{W}$ and its conjugate $\boldsymbol{W}^T$ are provided by the ASTRA Toolbox [13]. The iterative update of the reconstruction and motion parameters use independent stepsizes quantized by the Barzilai-Borwein stepsize formula [14] to accelerate the convergence:

$$\boldsymbol{x}^{k+1} = \boldsymbol{x}^k - \gamma_{\boldsymbol{x}}^k \nabla_{\boldsymbol{x}} f\left(\boldsymbol{x}^k, \boldsymbol{s}^k\right), \tag{10}$$

$$\boldsymbol{s}^{k+1} = \boldsymbol{s}^k - \gamma_{\boldsymbol{s}}^k \nabla_{\boldsymbol{s}} f\left(\boldsymbol{x}^k, \boldsymbol{s}^k\right), \tag{11}$$

with

$$\gamma_{\boldsymbol{x}}^k = \frac{\left\langle \boldsymbol{x}^k - \boldsymbol{x}^{k-1}, \nabla_{\boldsymbol{x}} f\left(\boldsymbol{x}^k, \boldsymbol{s}^k\right) - \nabla_{\boldsymbol{x}} f\left(\boldsymbol{x}^{k-1}, \boldsymbol{s}^{k-1}\right)\right\rangle}{\|\nabla_{\boldsymbol{x}} f(\boldsymbol{x}^k, \boldsymbol{s}^k) - \nabla_{\boldsymbol{x}} f(\boldsymbol{x}^{k-1}, \boldsymbol{s}^{k-1})\|_2^2}, \tag{12}$$

$$\gamma_{\boldsymbol{s}}^k = \frac{\left\langle \boldsymbol{s}^k - \boldsymbol{s}^{k-1}, \nabla_{\boldsymbol{s}} f\left(\boldsymbol{x}^k, \boldsymbol{s}^k\right) - \nabla_{\boldsymbol{s}} f\left(\boldsymbol{x}^{k-1}, \boldsymbol{s}^{k-1}\right)\right\rangle}{\|\nabla_{\boldsymbol{s}} f(\boldsymbol{x}^k, \boldsymbol{s}^k) - \nabla_{\boldsymbol{s}} f(\boldsymbol{x}^{k-1}, \boldsymbol{s}^{k-1})\|_2^2}. \tag{13}$$

The initial guess $\boldsymbol{x}^0$ of the reconstruction and $\boldsymbol{s}^0$ of the scaling parameters should be chosen so that they are as close to the true values as possible. Since the motion parameters are initialized with the values corresponding to the non-scaling phases (i.e., $\boldsymbol{s}^0 \equiv \boldsymbol{1}$), the initial reconstruction $\boldsymbol{x}^0$ corresponds to a reconstruction without scaling correction.

3 Validation

3.1 Phantom study

The simulation experiment uses a cylindrical bone scaffold of volume size $472 \times 480 \times 480$ (voxels) as a phantom. It is derived from a reconstruction by the gradient scheme (10) with the stepsizes quantized by (12) of real projection data of a bone scaffold in a static and uncompressed status, acquired by a TESCAN UniTOM XL Micro CT system. We consider 720 uniformly sampled cone beam projections over an angular range of $[0, 2\pi]$ radians. Gaussian noise with a standard deviation of 1% of the peak gray value of the projection data is added to the sinogram. The projections are captured at discrete angular time points and the motion is simulated as continuous constant scaling in all three dimensions y-z, x-z and x-y with the scaling factors range from 1 to 0.8, 0.86 and 1.25, respectively. The scaling estimation is restricted to consider just 10 time frames.

In order to quantify the study of the estimated scaling parameters, we consider the scaling model error:

$$\text{scaling model error} = \|\boldsymbol{s}_{\text{true}} - \boldsymbol{s}_{\text{estimated}}\|_2\,, \tag{14}$$

where $\boldsymbol{s}_{\text{true}}$ and $\boldsymbol{s}_{\text{estimated}}$ are the ground truth and estimated scaling parameters corresponding to all projection angles, respectively.

The convergence of the scaling estimation is achieved after around 150 iterations with the running time of 3 hours. The reconstruction results of the simulated projection data are shown in figure 2. The scaling estimation and the stability of the scaling model error are given in figure 3. The result of our method shows a clear improvement over the reconstructions without scaling correction.

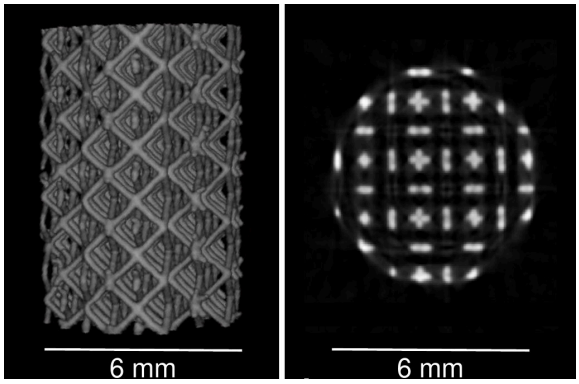

Figure 1: The bone scaffold (left) and an x-y cross-section slice of its (right).

3.2 Sponge dataset

The experiment considers a real scan of a soft sponge, acquired by the FleXCT system [15]. The scan includes two discrete stages, each consisting of 360 uniformly cone-beam projections equiangularly distributed in the range $[0, \pi]$ and the range $[\pi, 2\pi]$ of the first and second subscans, respectively. The original detector size is 1896×1920 (voxel), down-scaled onto the projection of the size 474×480 (voxel) by the binning number of 4. The sponge is compressed in the second stage with the corresponding scaling factors $(s_x, s_y, s_z) = (0.97, 0.93, 1.21)$. We use a reconstruction from a full angular range projection dataset of the sponge in the uncompressed status as a reference. The convergence of the scaling estimation is achieved after around 30 iterations with the running time of around 10 minutes. The reconstruction results are given in the figure 4.

4 Conclusion

In this work, we presented a method to simultaneously reconstruct a scaled object from a dynamic CT scan and estimate the corresponding scaling parameters. Our method performs well with both simulated and real projection data. However, the deformation on the real data is generally in local regions of the scanned object. Validations on real data acquired from locally-deformed objects will be performed in future research.

Author contributions

Anh-Tuan Nguyen and Jens Renders contributed equally to this work.

Acknowledgement

This research is supported by the Research Foundation-Flanders (FWO) (grant no. S007219N and grant no. 1SA2920N) and KU Leuven C2 project MAT-4D-XCT (grant no. 3E170432). The authors would like to thank Dr. Ehsan Nazemi and Dr. Zhihua

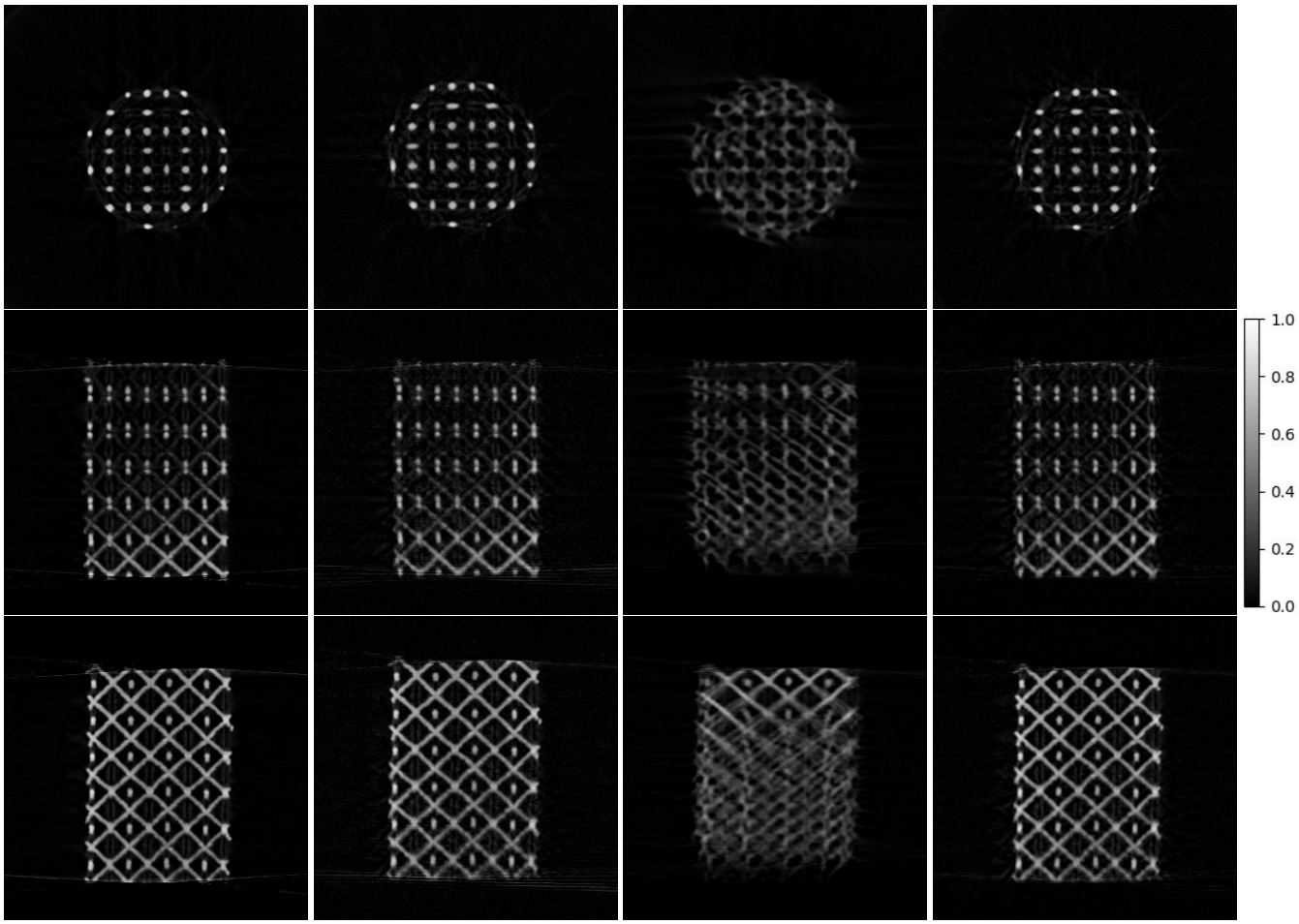

(a) Ground truth (b) Reconstruction with true scaling parameters (c) Reconstruction without scaling correction (d) Reconstruction with scaling correction

Figure 2: From top to bottom: x-y, x-z and y-z cross-sections of the reconstructions on the 3D bone scaffold.

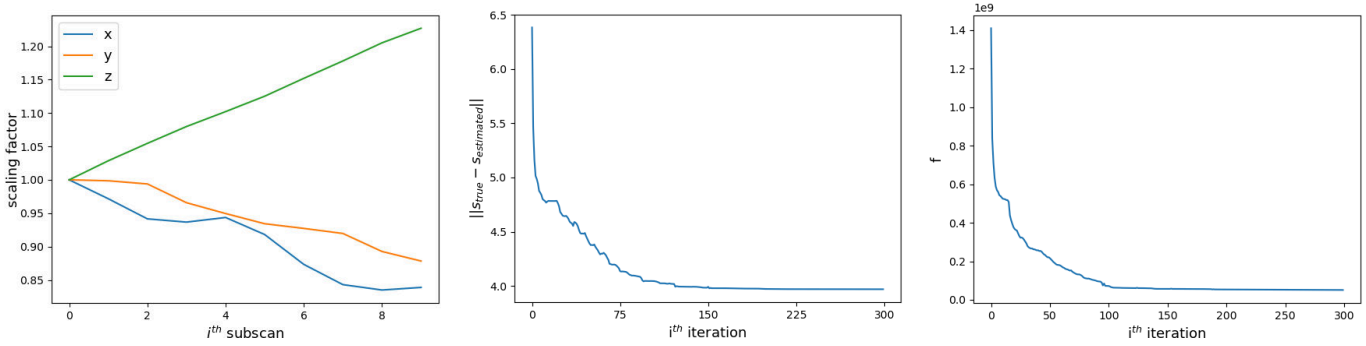

(a) Scaling estimation (b) l_2-norm scaling model error (c) objective function

Figure 3: The scaling estimation, scaling model error and objective function.

Liang for their support in creating the sponge's real projection data.

References

[1] J. Welzel, "Optical coherence tomography in dermatology: a review," *Skin Res. Technol.*, vol. 7, no. 1, pp. 1–9, 2001.

[2] M. W. Czabaj, M. L. Riccio, and W. W. Whitacre, "Numerical reconstruction of graphite/epoxy composite microstructure based on sub-micron resolution X-ray computed tomography," *Composites Science and Technology*, vol. 105, no. C, pp. 174–182, 2014.

[3] J. Renders, A.-T. Nguyen, J. De Beenhouwer, and J. Sijbers, "Motion compensating X-ray micro-CT of diamonds in a processing stage," in *31st International Conference on Diamond and Carbon Materials*, 2021.

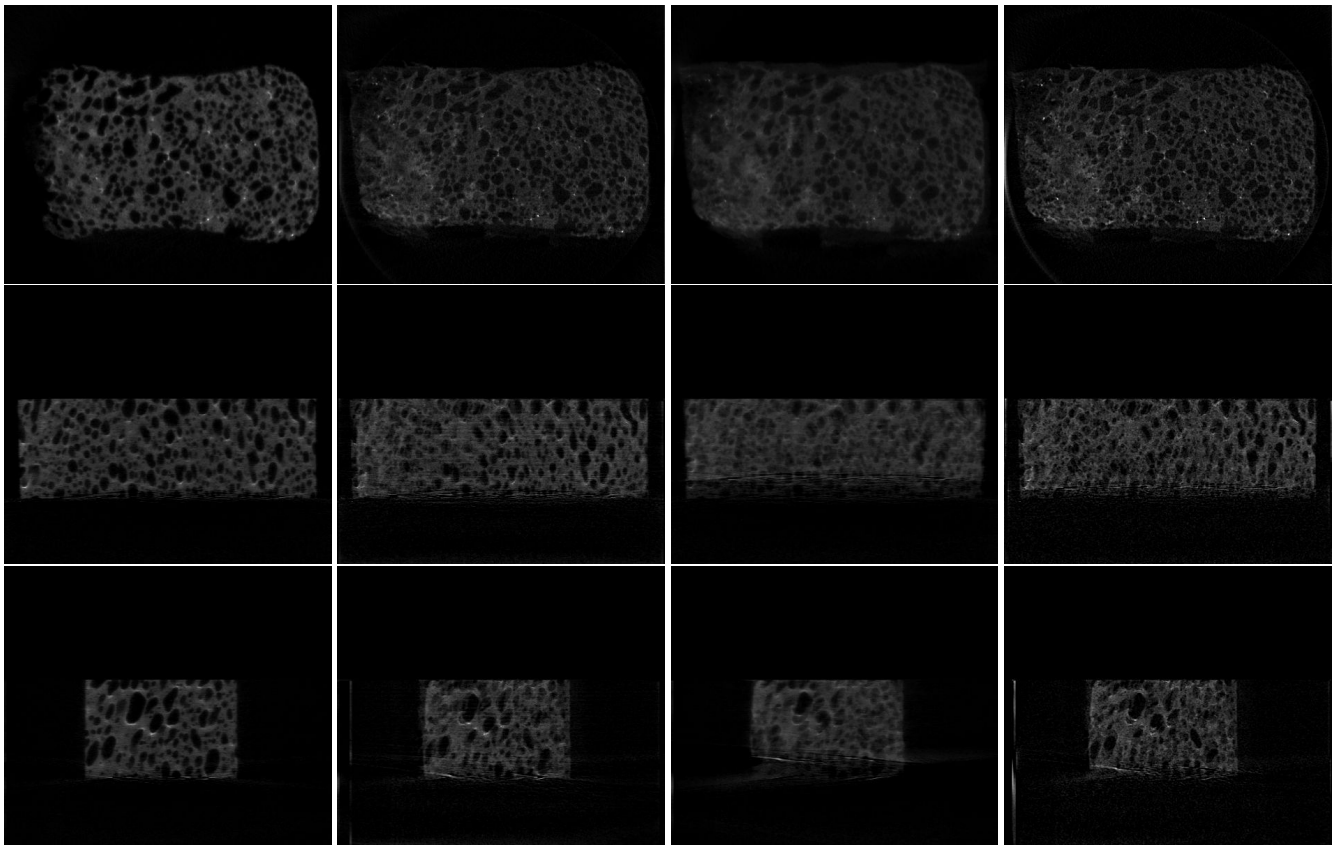

(a) Ground truth (b) Reconstruction with true scaling parameters (c) Reconstruction without scaling correction (d) Reconstruction with scaling correction

Figure 4: From top to bottom: x-y, x-z and y-z cross-sections of the reconstructions of the sponge.

[4] E. Y. Sidky and X. Pan, "Image reconstruction in circular cone-beam computed tomography by constrained total-variation minimization," *Phys. Med. Bio.*, vol. 53, pp. 4777–4807, 2008.

[5] H. Wu, A. Maier, R. Fahrig, and J. Hornegger, "Spatial-temporal total variation regularization (STTVR) for 4D-CT reconstruction," in *Proc. SPIE 8313, Medical Imaging 2012: Physics of Medical Imaging, 83133J*, 2012.

[6] G. Zang, R. Idoughi, R. Tao, G. Lubineau, P. Wonka, and W. Heidrich, "Space-time tomography for continuously deforming objects," *ACM Trans. Graph.*, vol. 37, no. 4, pp. 1–14, 2018.

[7] V. Van Nieuwenhove, J. De Beenhouwer, J. Vlassenbroeck, M. Brennan, and J. Sijbers, "MoVIT: A tomographic reconstruction framework for 4D-CT," *Optics Express*, vol. 25, no. 16, pp. 19236–19250, 2017.

[8] G. Van Eyndhoven, J. Sijbers, and J. Batenburg, "Combined motion estimation and reconstruction in tomography," in *Proceeding of the European Conference on Computer Vision (ECCV)*, 2012, pp. 12–21.

[9] M. Zehni, L. Donati, E. Soubies, Z. Zhao, and M. Unser, "Joint angular refinement and reconstruction for single-particle Cryo-EM," *IEEE Transactions on Image Processing*, vol. 29, pp. 6151–6163, 2020.

[10] R. Mooser, F. Forsberg, E. Hack, G. Székely, and U. Sennhauser, "Estimation of affine transformations directly from tomographic projections in two and three dimensions," *Machine Vision and Applications*, vol. 24, pp. 419–434, 2013.

[11] V. Van Nieuwenhove, J. De Beenhouwer, J. Vlassenbroeck, M. Brennan, and J. Sijbers, "MoVIT: A tomographic reconstruction framework for 4D-CT," *Optics Express*, vol. 25, no. 16, pp. 19236–19250, 2017.

[12] J. Renders, J. Sijbers, and J. De Beenhouwer, "Adjoint image warping using multivariate splines with application to 4D-CT," *Medical Physics*, vol. 48, no. 10, pp. 6362–6374, 2021.

[13] W. van Aarle, W. J. Palenstijn, J. De Beenhouwer, T. Altantzis, S. Bals, K. J. Batenburg, and J. Sijbers, "The ASTRA Toolbox: A platform for advanced algorithm development in electron tomography," *Ultramicroscopy*, vol. 157, pp. 35–47, 2015.

[14] J. Barzilai and J. Borwein, "Two-point step size gradient methods," *IMA Journal of Numerical Analysis*, vol. 8, no. 1, pp. 141–148, 1988.

[15] B. De Samber, J. Renders, T. Elberfeld, Y. Maris, J. Sanctorum, N. Six, Z. Liang, J. De Beenhouwer, and J. Sijbers, "FleXCT: a flexible X-ray CT scanner with 10 degrees of freedom," *Optics Express*, vol. 29, no. 3, pp. 3438–3457, 2021.